Effect of cooling mediums on mechanical properties and wear behaviour of binary β-type Ti-Mo alloy for bio-implant applications

Mukhethwa Netshia[1, 3*], *Maje* Phasha[2], *Bongani* Ngobe[2], and *Peter* Olubambi[3]

[1*]Pyrometallurgy Division, Mintek, Private Bag X 3015, Randburg 2125, South Africa, MukhethwaN@mintek.co.za
[2]Advanced Materials Division, Mintek, Private Bag X 3015, Randburg 2125, South Africa, MajeP@mintek.co.za, bonganing@mintek.co.za
[3]Centre for Nanoengineering and Advanced Materials, School of Mining, Metallurgy and Chemical Engineering, University of Johannesburg, P.O. Box 17011, Doornfontein 2028, South Africa, mukheathwa@gmail.com, polubambi@uj.ac.za

Abstract. Orthopaedic implants are increasingly used to correct skeletal dysfunctions by replacing or repairing damaged bone tissue with appropriate biomaterials. This study investigates the effect of cooling medium on the mechanical properties and wear behaviour of the solution heat-treated β-type Ti-Mo alloy. Samples were solution heat-treated at 900°C and cooled in different cooling media, such as water quenching, air, and furnace cooling. The phases, morphology, and microstructural analyses were performed using X-ray diffraction (XRD), optical microscope, and electron backscatter diffraction (OM and EBSD). The mechanical and nanomechanical properties of the alloys were analysed using Vickers hardness and nanoindentation machines. The wear test analyses of the alloys were conducted using a tribometer. XRD and microstructural characterization showed the crystalline phase, and the microstructure of the alloys was affected by the cooling medium. The furnace-cooled sample yielded high micro-hardness (454 HV) due to the grain refinement attributed to the presence of α phase.

Corresponding author: MukhethwaN@mintek.co.za, Mukheathwa@gmail.com

1 Introduction

The population of the elderly is rising in many countries worldwide, leading to an increased demand for artificial implants due to the number of hard-tissue failures experienced. This situation necessitates further research to find metals and alloys suitable for manufacturing implant devices. Creating and investigating novel alloys that exhibit local and systemic biocompatibility and suitable mechanical properties is essential. Alloys utilized as biomaterials have recently undergone extensive review [1]. Due to their exceptional corrosion resistance, biocompatibility, and great strength under static and dynamic loading

situations, titanium alloys are the best material for large load-bearing implants [2]. Ti-6Al-4V alloy is frequently used as an implantable material [3]. However, the unfavourable features that limit the application are their possible hazards during long-term implantation and high Young's modulus [4].

In the early 1980s, large quantities of titanium (Ti), vanadium (V), and aluminium (Al) black waste were identified in surrounding tissues under excessive wear, such as knee and modular head components. Although no harmful consequences have been attributed to this black debris, safety concerns concerning vanadium and aluminium have been highlighted in the literature [5]. Several alloying elements are currently being explored to replace V and Al. Among alloying elements currently under investigation, beta (β) stabilizing elements are preferred alloys suitable for bioimplant applications [6]. The identified suitable β-stabilizers are mainly comprised of refractory elements such as molybdenum (Mo), niobium (Nb), tantalum (Ta), etc. Among these elements, Mo is considered one of the most effective β-stabilizing alloying elements compared to V, chromium (Cr), iron (Fe), copper (Cu), tantalum (Ta), and niobium (Nb). Moreover. Mo is eight times less expensive than V [3, 7].

Various studies have been done on the Ti-Mo system. Among studies conducted on Ti-Mo systems, numerous works have been devoted to Ti-4Mo, Ti-8Mo, Ti-10Mo, and Ti-15Mo systems. However, these systems suffer from poor mechanical and wear properties. Mechanical properties of titanium alloys can be markedly enhanced through heat treatment, which induces considerable alterations in phase composition and microstructure, including grain sizes, shapes, orientation distribution, and the morphology of phase constituents within the grains, during the subsequent phase transformations α↔β. Significant work has been devoted to devising novel methods for the thermal treatment of these materials, aiming to achieve alternative microstructures that offer an improved balance of mechanical properties [8]. This study investigates the effect of cooling rate on the newly developed binary Ti-14Mo alloy.

2 Materials and methods

2.1 Material preparation

A 30g binary Ti-14Mo alloy ingot was produced using a state-of-the-art button arc melting machine. During the melting process, commercially available high-purity titanium (Ti) and molybdenum (Mo) metallic powders were considered. The arc melting machine was equipped with a tungsten electrode and a water-cooled copper (Cu) hearth, operating under a controlled argon (Ar) atmosphere to prevent oxidation. Before melting the Ti-14Mo alloy's ingot, pure titanium was melted to capture any excess oxygen within the chamber. To ensure complete chemical homogeneity, the ingot was flipped and remelted three times. This approach ensured uniform distribution of alloying elements throughout the ingot, achieving the desired composition and properties.

2.2 Heat treatment experiment

Three representative samples were sectioned from the Ti-14Mo ingot and labeled according to their respective heat treatment procedures, as represented in Table 1.

Table 1. The investigated samples and their respective heat treatment procedures.

Sample ID	Composition (Wt.%)	Heat treatment	Cooling medium
Sample A	Ti-14Mo	900°C	Water quench
Sample B	Ti-14Mo	900°C	Air cooling
Sample C	Ti-14Mo	900°C	Furnace cooling

The experimental heat treatment was conducted using a Lento® muffle furnace under an argon (Ar) controlled atmosphere to ensure oxidation is prohibited. The heat-treatment process was carried out for 1 hour at temperatures set to 900˚C for Samples A, B, and C, respectively. Thereafter, the samples were rapidly quenched in water (WQ), air-cooled (AC), and furnace-cooled (FC) to retain the microstructures attained at the respective heat treatment medium. The heat-treated samples were then mounted and labeled, respectively, as shown in Table 1. Below is the solution heat treatment graph (Fig. 1), illustrating how the samples were heat-treated.

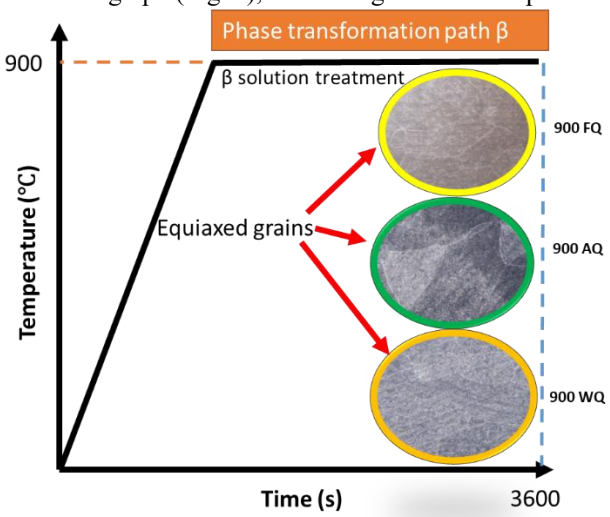

Fig. 1. Solution treatment procedure.

2.3 Microstructure and XRD characterization

The mounted samples were grinded with SiC papers to a 1200 grit surface finish and mechanically polished to 1µm surface finish. The polished surfaces were etched in a Kroll's reagent (2% HF + 6% HNO3 + 92% H2O) to reveal the developed microstructures. Microstructural analysis was performed using Olympus DSX510 optical microscope (OPM) and a Zeiss Cross Beam 540 equipped with an Oxford Instrument Nordlys Max3 Electron Backscatter Diffraction (EBSD) camera. To ensure accurate detection of phases present, a Bruker D8® X-Ray Diffractometer (XRD) equipped with a Co-Kα source (λ=1.78897 Å) operating in Bragg-Brentano geometry was used and operating at room temperature.

2.4 Mechanical testing

A DuraVision micro-Vickers hardness tester was used to evaluate the hardness of the samples. Random indentations were made on the prepared surfaces using a load of 3kg. The

nano-mechanical properties, such as elastic modulus (E), yield stress (σy), and yield strain (εy), were determined using a nanoindentation tester (Anton Paar Hit 300). The diamond Berkovich tip with a radius curvature of 2µm was used in the testing, with a loading force of 500 mN, loading and unloading rate of 6000 mN/min, and holding of 10s. To ensure reliability and precision, more than four indentations were conducted for each sample.

2.5 Wear test

The wear behavior of the alloys was evaluated using a tribometer pin-on-disk (TRB^3 by Anton Paar) friction module approach under dry conditions. An Alumina ceramic ball of 6 mm diameter was used as a counterface material that slides against the samples. A contact force of 10 N and a spindle speed of 2.17 cm/s were performed in ambient conditions. The wear test of the solution heat-treated samples was analyzed as a function of sliding time, and the coefficient of friction for each material was reported. The wear rates were determined using a profilometer. The following equations were utilized to calculate the wear rate.

The wear rate (W) was calculated using Archard's linear wear equation:

$$W = KF_N \qquad \textit{Equation 1}$$

Where K is the wear coefficient, and F_N is the applied load. K is calculated using the relation:

$$K = \frac{3HV}{F_N D} \qquad \textit{Equation 2}$$

HV is the Vickers hardness of the softer body in contact, and D is the sliding distance.
Finally, the specific wear rate, k, was determined based on the Lancaster relationship, where V is the volume loss:

$$K = \frac{V}{F_N \times D} \qquad \textit{Equation 3}$$

3 Results and discussion

3.1 Phase composition after solution heat treatment

XRD patterns of the solution heat-treated samples are shown in Fig. 2. The solution-treated samples mainly consist of body-centered cubic (BCC), hexagonal close packed (HCP), and martensitic orthorhombic (α″) crystal structures. All samples were solution treated above the β transus temperature. The β transus is the temperature range at which titanium alloys shift from a microstructure mostly consisting of the α-phase to one that is mainly β-phase (BCC) [9, 10]. For the considered alloy, the β transus temperature ranges between 700–1050°C.
It is evident from Fig. 2 that when Ti-14Mo alloy is subjected to WQ and AC from 900°C, it results in β+α″ phases. The presence of α″ martensitic phase is attributed to the diffusionless martensitic transformation from β phase. However, when the alloy is allowed to undergo self-cooling in the furnace, it is comprised of HCP and BCC (α+β) phases. Current results are consistent with the literature, which states that when Mo content is ≥10 wt.%, the β-phase becomes the dominant phase [11, 12]. Furthermore, in accordance with the Ti-Mo phase diagram, when Cp-Ti is alloyed with 14 wt.% of Mo and heat treated at 900°C, the β phase becomes stable. Although other studies reported the formation of athermal (ω) phase, this deleterious phase is not observed in the current study [12, 13]. The peak intensity of β phase is much higher in the WQ sample than in the AC and FC samples, an indication of high β retention under this heat treatment procedure. Similar phases were also observed in Ti-12Mo and Ti-18Mo alloys, whereby the transformation of α″ phases was observed upon water quenching [14, 15]. It is worth noting that the intensity α″ phase is much higher in air cooled sample compared to the WQ sample. It thus follows from these results that the precipitation

of α″ phase is strongly influenced by the cooling medium. Slow cooling rates (furnace cooling) favor the precipitation of the α phases from the β phase field. Similar phases were also observed in Ti-12Mo and Ti-18Mo, where the precipitation of α phase was observed as the alloys were cooled inside the furnace [14, 15]. The formation of the α phases is owed to the eutectoid diffusion reaction [16, 17]. This results in finely dispersed alpha phases forming in the retained beta phase [8].

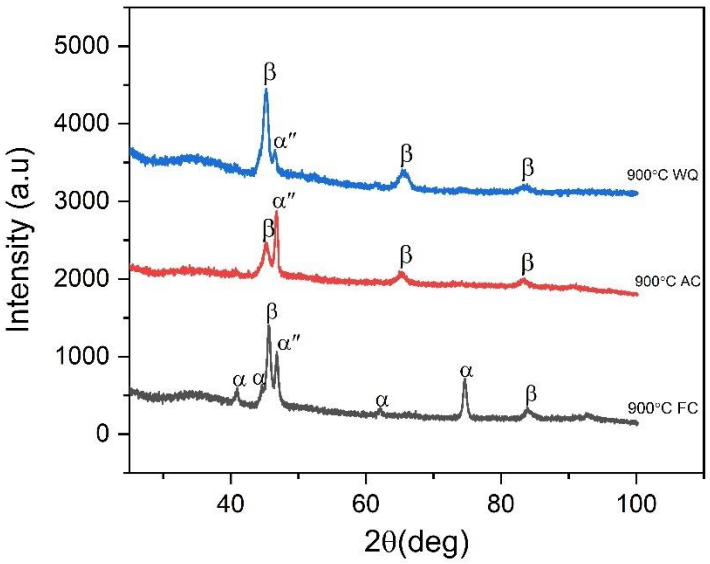

Fig. 2. XRD patterns of the solution heat-treated samples.

3.2 Microstructural properties after solution heat treatment

3.2.1 EBSD analysis

The grain and orientation mapping of the samples are shown in Fig. 3. All the samples are characterized by equiaxed large and small grains. The WQ sample in Fig. 3 (a) is mainly comprised of equiaxed large and small grains, while the AC sample in Fig. 3 (b) and the FC samples in Fig. 3 (c) exhibit large and small longitudinal grains, respectively. Grains within all the samples are uniformly distributed and have no preferred orientation. It has been reported that it is very difficult to refine the initial large β-grain microstructure after the α→β transformation [18]. The retainment of large grains after water quenching in Fig. 3 (a) confirms what has been reported upon the α→β transformation. However, grain growth and refinement occurred as the alloy was AC in Fig. 3 (b). This observation is in agreement with the reported view that once the large β-grain microstructure is established, it cannot be diminished by further heat treatments [18]. During cooling, the alloy tends to transform from β→α/α″ depending on how fast the alloy is cooled. It is also evident that grain sizes became larger upon air cooling compared to the WQ sample. It has been reported that recrystallization and growth are expected to occur upon FC or normalizing heat treatment processes of Ti alloys [19, 20]. However, as the alloy was slowly cooled inside the furnace, the grains became smaller compared to WQ and AC. This grain refinement observed in Fig. 3 (c) is associated with the β→α transformation.

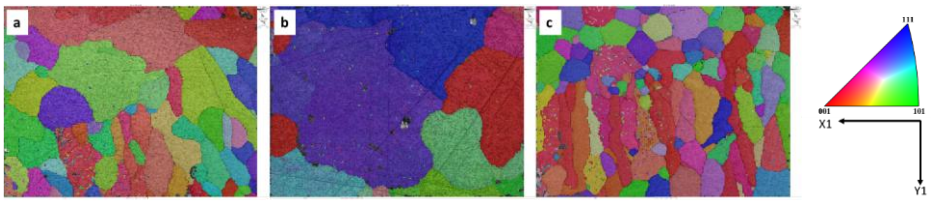

Fig. 3. Grains and orientation analysis of Ti-14Mo (a) water quenched, (b) air cooling, (c) furnace cooling.

Fig. 4 shows the grain size distribution graph indicating how large and small grains are distributed. The grain size distribution corroborates the results obtained in Fig. 3. The WQ sample in Fig. 4 (a). The FC samples in Fig. 4 (c) have a similar distribution, whereby medium and smaller grain sizes dominate. In contrast, the AC samples in Fig. ***4*** (c) have a less medium and smaller grain size distribution than the other two.

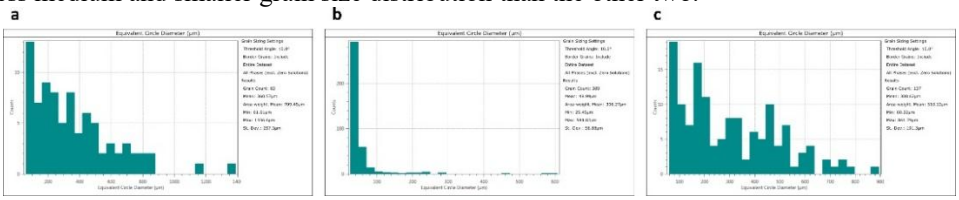

Fig. 4. Grain size distribution graph (a) water quenched, (b) air cooling, (c) furnace cooling

3.2.2 Optical microscope analysis

The optical microstructures of the solution heat-treated samples are shown in Fig. 5. The micrographs reveal the effect of heat treatment on the microstructures of the alloys. Small grain boundaries were observed on all microstructures. Large equiaxed grains were observed in Fig. 5 (b), where the sample was heat treated at 900°C and AC, while Fig. 5 (a & c) revealed medium and small equiaxed grains where the samples were heat treated at 900°C followed by WQ and AC. Similar grains to those in Fig. 5 (a & c) were also observed in past studies [13, 19, 21]. The small and large grains observed in Fig. 5 corroborate those obtained in Fig. ***3***. Current studies indicate that the dissolution of the primary α-phase results in immediate grain growth of β microstructure during solution treatment [18]. However, it was revealed in Fig. 2 that during WQ, there was the transformation of β-phase to martensite ($\beta \rightarrow \alpha''$), resulting in grain size getting refined into smaller grains as the material gets hardened due to the formation of martensite (α''). The AC alloy in Fig. 5 (b) reveals micrographs with large, elongated grain sizes and small grain boundaries. The large size of the grains can be ascribed to the great driving force for grain growth at high temperatures [22]. According to the literature, large-grain structures are expected to form during normalizing or AC [20]. However, small grain sizes were observed upon FC in Fig. 4 (c). The large grain sizes observed in Fig. 5 (c) indicate grain refinement owed to eutectic formation of harder α phase.

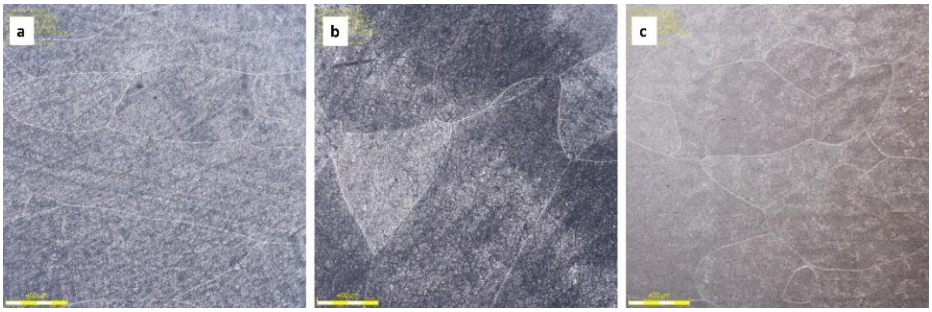

Fig. 5: Shows the optical microscope images solution of heat-treated Ti-14Mo alloys at 900°C, followed by (a) water quenched, (b) air cooling, and (c) furnace cooling.

3.3 Mechanical properties and wear performance

3.3.1 Micro-hardness and nanoindentation

Fig. 6 shows the Vickers hardness results of the heat-treated alloys. The hardness profile shows a decrease in hardness during AC compared to the WQ sample and an increased hardness for the FC sample. Increased hardness in the FC sample is attributed to β→α eutectic transformation, in which the formation of harder α phase resulted in refined grains, as shown in Fig. 2, Fig. 3 (c), and Fig. 5 (c). The larger the grain, the higher the grain boundary area, inhibiting the dislocation movement, resulting in high hardness and good strength [23]. The decrease in hardness during AC is associated with the grain growth observed in Fig. 3 (b) and Fig. 5 (b). Large grains tend to promote the movement of dislocation and low grain boundary areas, resulting in low or poor hardness. In titanium alloys, it is well known that the ω phase has the highest hardness value, followed by α, α′, α″, and β phases [24, 25]. As the WQ sample is characterized by β and α″ phases observed in Fig. 2, the alloy is expected to harden due to martensitic transformation (α″). The precipitation of α″ in the quenched sample didn't affect the hardenability of the alloy compared to the FC sample.

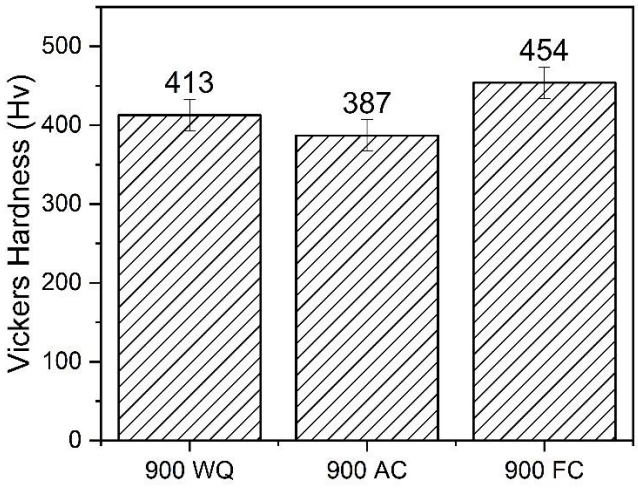

Fig. 6. Vickers hardness of the heat-treated sample

The nanomechanical properties of the heat-treated samples are presented in Table 2. The WQ and FC samples have properties similar to those of the AC sample. The Young's

modulus, yield stress, and yield strain of the WQ and FC samples are lower than the AC sample. The decrease in Young's modulus, yield stress, and yield strain of the WQ and the FC samples is attributed to the presence of the β-phase, which is dominant in the WQ samples and the presence of the orthorhombic α″ martensite in FC samples as observed in Fig. 2. The increase in Young's modulus, yield stress and yield strain during AC could be associated with the precipitation of α/α′ and α″ martensite and large equiaxed α/α′ + α″ grains as observed in Fig. 2, Fig. 3, and Fig. 5. According to the literature, Young's modulus of bone implants should be closer to that of a human bone (10-40 GPa) [21, 26, 27]. Table 2 shows that the water-quenched and the FC samples possess a lower Young's modulus of 70 GPa, closer to human bone. Studies indicate that commercially pure titanium Cp-Ti possesses a Young's modulus of 102.7 GPa and a yield stress of 275 MPa [28-30]. Adding 14 wt.% of Mo to Cp-Ti and ST, the alloy within the β transus temperature lowered Young's modulus and increased the yield stress and strain. It has been reported that adding Mo to Ti will stabilize a beta phase in Ti and decrease Young's modulus [31-33]. The results in Table 2 confirm the results obtained in Fig. 2 and Fig. 5.

Table 2: Nanomechanical properties of the heat-treated samples

Heat treatment (°C) and cooling medium	Young's modulus (GPa)	Yield stress (MPa)	Yield strain (MPa)
900 WQ	70	419	0.01
900 AC	103	2261	0.02
900 FC	70	425	0.01

Fig. 7 displays the load-displacement curves of the ST samples. It was observed that all the samples exhibited elastic-plastic behaviour. For elastic-plastic materials, the unloading path does not follow the loading path as it would for a perfectly elastic material, and there is an observable hysteresis denoted by the area between the loading and unloading path [34, 35]. The loading and unloading displacement of WQ and AC samples follows the same trend, confirming the yield stress and strain obtained in Table 2. Depth penetration of the indentation for the two samples (WQ and FC) is around ~2200 nm at a maximum load of 500 mN. The depth penetration similarity indicates that the two samples behave similarly regarding elastic-plastic deformation behaviour. However, the loading and unloading displacement of the FC differs from the rest. The unique behaviour of the AC sample is associated with the high yield stress and yield strain obtained in Table 2. The depth penetration of the indentation is around ~2000 nm at a maximum load of 500 mN, suggesting that the material (AC sample) can deform much better than the rest of the samples. The deformation behaviour illustrated in Fig. 7 confirms the nanomechanical properties of the samples in Table 2. WQ and FC samples have better Young's modulus than the AC sample for bioimplant application.

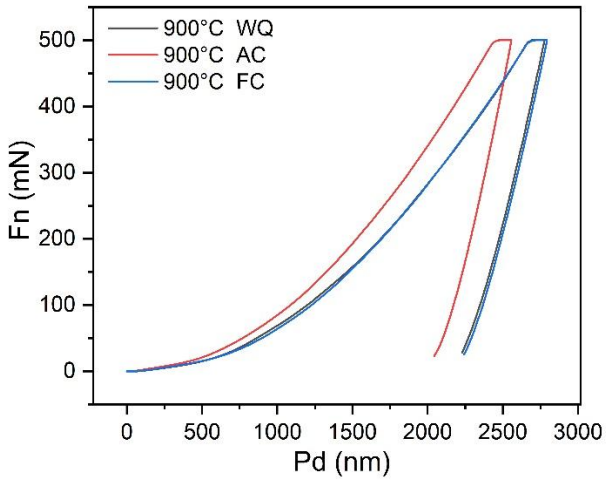

Fig. 7. Load-unload curves of heat-treated samples

3.3.2 Wear behaviour

Fig. 8 shows the friction coefficient concerning time graphs for all the samples obtained from the tribometer at a load of 10 N under dry (atmospheric) conditions. The graphs reveal fluctuation of COF for all the samples throughout the sliding time. This behaviour can be attributed to localized material fractures and debris removal on the worn surface during dry sliding [36]. It was observed that the FC and AC samples exhibit a high friction coefficient and follow the same COF trend. The WQ sample shows a lower COF than the AC and FC samples. According to the literature, it has been previously stated that high COF results in a high wear rate, while low COF results in a low wear rate [37]. However, no one has established a mathematical relation between the COF and wear rate, although this is widely recognized [38].

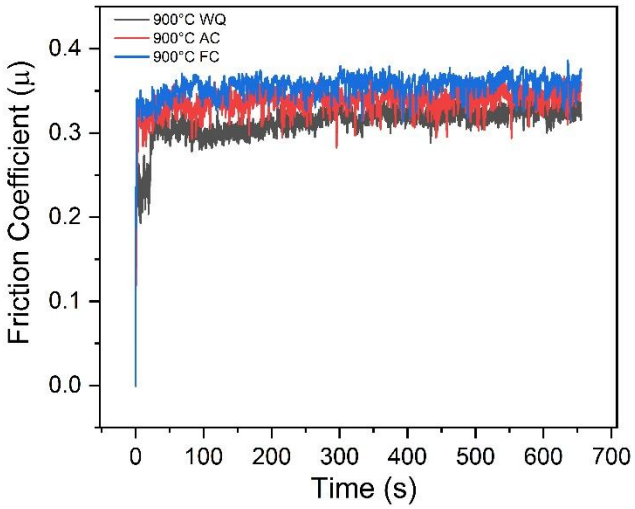

Fig. 8. Friction coefficient of the heat-treated samples

The results of the wear rate in Fig. 9 were determined using a profilometer. The calculations were based on $W = K F_N$ *Equation 1* $K = \frac{V}{F_N \times D}$ *Equation 3*. The wear

rate of the three alloys was observed, ranging from 1.15-2.48x10^{-3}mm^{3}N.m. As expected, the FC sample exhibits a lower wear rate than the WQ and AC samples. The wear rate trend confirms the Vickers hardness obtained in Fig. 3, which corroborates the grain size obtained in Fig. ***3*** and Fig. 5. It has been reported that high hardness tends to result in a high wear rate [39]. The small grains observed in Fig. ***3*** (c) and Fig. 5 (c) tend to inhibit the dislocation movement and increase the grain boundary area, resulting in high hardness and a lower rate.

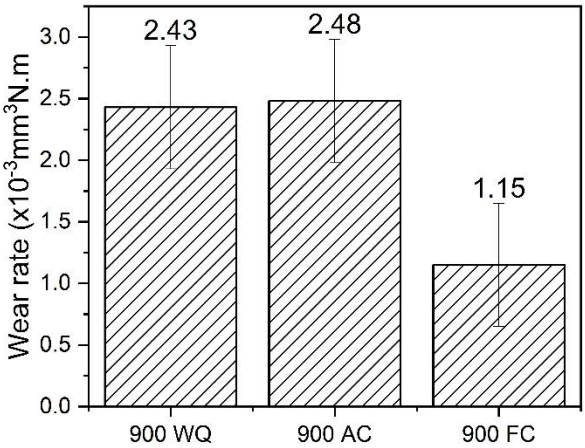

Fig. 9. Wear rate of the heat-treated samples

3.3.3 Wear morphology

The heat-treated sample's wear surfaces were characterized to elucidate the wear mechanism. The characterization results are shown in Fig. 10. The wear morphologies of the ST samples exhibited a relatively similar worn surface, including significant abrasion (marked with a yellow arrow) and continuous abrasive furrows (white arrow). Notably, the furrows were aligned parallel to the sliding direction, indicating a typical morphology of abrasive wear. It is worth noting that the FC sample differs from the other two samples, with no clear furrows and wear debris, suggesting less abrasive wear during the wear test than the other two samples. The surface morphology in Fig. 10 (c) also confirms the results obtained in Fig. 9, whereby a low wear rate was determined. Fig. 10 (b) reveals more abrasive wear morphology than Fig. 10 (a). This confirms the results obtained in Fig. 9. Fig. 10 (b) encountered more abrasive wear damage than Fig. 10 (a) and (c). The confirmation of results obtained in Fig. 9 indicates that the FC sample has a better wear behaviour compared to the rest of the samples.

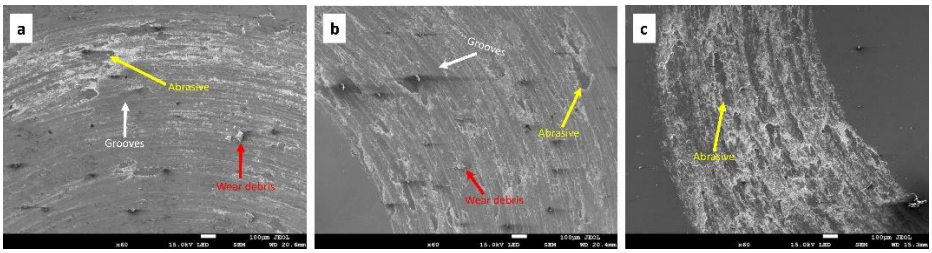

Fig. 10. SEM micrographs illustrating the wear morphology of the heat-treated samples at 900°C (a) water quench, (b) air cooling, and (c) furnace cooling

4 Conclusion

The results detailed above lead to the following conclusions:

- The results presented in this paper conclude that the cooling medium influenced the alloys' mechanical properties and wear behaviour.
- XRD and microstructural characterization showed the crystalline phase, and the microstructure of the alloys was affected by the cooling medium. A BCC matrix crystal structure and precipitation of the HCP crystal structure within the matrix characterize the alloys. A metastable β-titanium was captured during water quenching with the presence of martensitic α'' phase. Similarly, diffusionless $\beta \rightarrow \alpha''$ martensitic transformation was observed during furnace cooling, resulting in grain refinement.
- The furnace-cooled sample yielded high micro-hardness due to the grain refinement attributed to the presence of the α phase.
- The wear rate and the wear behaviour of the furnace-cooled samples confirm the martensitic transformation and grain refinement. The furnace-cooled sample's wear rate was low due to high hardness and large grains caused by a larger volume fraction of harder α phase.

The authors would like to acknowledge the financial support of the National Research Foundation-South Africa, Advanced Materials Division-Mintek, and Pyrometallurgy Division-Mintek.
Data availability: Data will be made available on request.

References

1. N. Oliveira and A. C. Guastaldi, Electrochemical behavior of Ti–Mo alloys applied as biomaterial. Corros. Sci. **50**(4): p. 938-945(2008)
2. A. Almeida, et al., Laser-assisted synthesis of Ti–Mo alloys for biomedical applications. Mater. Sci. Eng. **32**(5): p. 1190-1195(2012)
3. J. Gupta, S. Ghosh, and S. Aravindan, Effect of Mo content on Ti-Al-Mo ternary alloys for biomedical applications. Materials Letters. **305**: p. 130865(2021)
4. H. Liu, et al., Microstructure, mechanical properties and corrosion behaviors of biomedical Ti-Zr-Mo-xMn alloys for dental application. Corros. Sci. **161**: p. 108195(2019)
5. N. Eliaz, Corrosion of metallic biomaterials: a review. Materials. **12**(3): p. 407(2019)
6. P. Pesode and S. Barve, A review—metastable β titanium alloy for biomedical applications. J. Eng. Appl. Sci. **70**(1): p. 25(2023)
7. F. Xie, et al., Selective laser sintered porous Ti–(4–10) Mo alloys for biomedical applications: Structural characteristics, mechanical properties and corrosion behaviour. Corros. Sci. **95**: p. 117-124(2015)
8. S. Ankem and C. Greene, Recent developments in microstructure/property relationships of beta titanium alloys. J. Mater. Eng. **263**(2): p. 127-131(1999)
9. Y. Niu, et al., Machine learning-based beta transus temperature prediction for titanium alloys. J. Mater. Res. Technol. **23**: p. 515-529(2023)
10. I. Mendoza, D. Villalobos, and B. Alexandrov, Crack propagation of Ti alloy via adiabatic shear bands. J. Mater. Eng. **645**: p. 306-310(2015)
11. W. Ho, C. Ju, and J. C. Lin, Structure and properties of cast binary Ti–Mo alloys. Biomaterials. **20**(22): p. 2115-2122(1999)
12. M. Netshia, et al. Characterization of the solution heat-treated binary β-type Ti-Mo alloy for bio-implant applications. in *MATEC Web of Conferences*. 2024. EDP Sciences.

13. P. S. Nnamchi, et al., Mechanical and electrochemical characterisation of new Ti–Mo–Nb–Zr alloys for biomedical applications. J. Mech. Behav. Biomed. Mater. **60**: p. 68-77(2016)
14. Z. ZC, et al., The Atomic Defect Relaxation Processes in the Ti–Mo Alloys. Materials Transactions. **61**(6): p. 1051-1057(2020)
15. F. Sun, F. Prima, and T. Gloriant, High-strength nanostructured Ti–12Mo alloy from ductile metastable beta state precursor. J. Mater. Eng. **527**(16-17): p. 4262-4269(2010)
16. Y. Zheng, et al., Role of ω phase in the formation of extremely refined intragranular α precipitates in metastable β-titanium alloys. Acta Mater. **103**: p. 850-858(2016)
17. Y. Zheng, et al., The indirect influence of the ω phase on the degree of refinement of distributions of the α phase in metastable β-Titanium alloys. Acta Mater. **103**: p. 165-173(2016)
18. O. M. Ivasishin and R. V. Teliovich, Potential of rapid heat treatment of titanium alloys and steels. J. Mater. Eng. **263**(2): p. 142-154(1999)
19. P. Yadav and K. K. Saxena, Effect of heat-treatment on microstructure and mechanical properties of Ti alloys: An overview. Materials Today: Proceedings. **26**: p. 2546-2557(2020)
20. B. Mintz, Influence of cooling rate from normalizing temperature and tempering on strength of ferrite–pearlite steels. Metals Technology. **11**(1): p. 52-60(1984)
21. Z. Guo, et al., Ti–Mo–Zr alloys for bone repair: mechanical properties, corrosion resistance, and biological performance. J. Mater. Res. Technol. **24**: p. 7624-7637(2023)
22. P. Ji, et al., Controlling the corrosion behavior of Ti-Zr alloy by tuning the α/β phase volume fraction and morphology of β phase. J. Alloys Compd. **825**: p. 154153(2020)
23. J. Hu, et al., Grain boundary stability governs hardening and softening in extremely fine nanograined metals. Science. **355**(6331): p. 1292-1296(2017)
24. P. A. B. Kuroda, et al., The Effect of Solution Heat Treatment Time on the Phase Formation and Selected Mechanical Properties of Ti-25Ta-x Zr Alloys for Application as Biomaterials. JMEP. **30**(8): p. 5905-5913(2021)
25. P. A. B. Kuroda, et al., The Effect of Solution Heat Treatment Temperature on Phase Transformations, Microstructure and Properties of Ti-25Ta-x Zr Alloys Used as a Biomaterial. JMEP. **29**: p. 2410-2417(2020)
26. M. Niinomi, et al., Biomedical titanium alloys with Young's moduli close to that of cortical bone. Regen. Biomater. **3**(3): p. 173-185(2016)
27. A. Brizuela, et al., Influence of the elastic modulus on the osseointegration of dental implants. Materials. **12**(6): p. 980(2019)
28. H. Y. Um, et al., Mechanical and biological behavior of ultrafine-grained Ti alloy aneurysm clip processed using high-pressure torsion. J. Mech. Behav. Biomed. Mater. **68**: p. 203-209(2017)
29. A. W. Nugroho, Investigation of the production and mechanical properties of porous Beta Titanium alloy compacts prepared by powder metallurgy processes for biomedical applications. 2013, Curtin University(2013)
30. F. Arias-González, et al., Laser-deposited beta type Ti-42Nb alloy with anisotropic mechanical properties for pioneering biomedical implants with a very low elastic modulus. Materials. **15**(20): p. 7172(2022)
31. X. Zhao, et al., Beta type Ti–Mo alloys with changeable Young's modulus for spinal fixation applications. Acta Biomater. **8**(5): p. 1990-1997(2012)
32. W.-d. Zhang, et al., Elastic modulus of phases in Ti–Mo alloys. Mater. Charact. **106**: p. 302-307(2015)

33. M. G. de Mello, et al., The effect of Sn addition on phase stability and phase evolution during aging heat treatment in Ti–Mo alloys employed as biomaterials. Mater. Charact. **110**: p. 5-13(2015)
34. K. Wahl and S. S. Asif, Surface mechanical measurements at the nanoscale, in *Adhesion Science and Engineering*. Elsevier. p. 193-220(2002)
35. S. E. Arevalo, D. M. Ebenstein, and L. A. Pruitt, A methodological framework for nanomechanical characterization of soft biomaterials and polymers. J. Mech. Behav. Biomed. Mater. **134**: p. 105384(2022)
36. A. Meng, et al., Tribo-induced microstructural changes and associated wear mechanisms of CoFeNi2 medium entropy alloy at elevated temperatures. Tribology International. **189**: p. 108892(2023)
37. J. A. Williams, Wear modelling: analytical, computational and mapping: a continuum mechanics approach. Wear. **225**: p. 1-17(1999)
38. H. Czichos, Tribology: a systems approach to the science and technology of friction, lubrication, and wear. Vol. 1. Elsevier(2009)
39. J. Hawk, et al., Laboratory abrasive wear tests: investigation of test methods and alloy correlation. Wear. **225**: p. 1031-1042(1999)